Received: 24 March 2023 | Revised: 27 June 2023 | Accepted: 28 June 2023

DOI: 10.1002/rra.4186

RESEARCH ARTICLE

WILEY

Automated fluvial hydromorphology mapping from airborne remote sensing

Richard D. Hedger | Marie-Pierre Gosselin

Norwegian Institute for Nature Research – NINA, Trondheim, Norway

Correspondence
Richard D. Hedger, Norwegian Institute for Nature Research – NINA, P.O. Box 5685 Torgard, NO-7485 Trondheim, Norway.
Email: richard.hedger@nina.no

Funding information
FME HydroCen: Norwegian Research Centre for Hydropower Technology; Norwegian Institute for Nature Research (NINA)

Abstract

Mapping fluvial hydromorphology is an important part of defining river habitat. Mapping via field sampling or hydraulic modeling is however time consuming, and mapping hydromorphology directly from remote sensing data may offer an efficient solution. Here, we present a system for automated classification of fluvial hydromorphology based on a deep learning classification scheme applied to aerial orthophotos. Using selected rivers in Norway, we show how surface flow patterns (smooth or rippled surfaces vs. standing waves) can be classified in imagery using a trained convolutional neural network (achieving a training and validation accuracy of >95%). We show how integration of these classified surface flow patterns with information on channel gradient, obtained from airborne topographic LiDAR data, can be used to compartmentalize the rivers into hydromorphological units (HMUs) that represent the dominant flow features. Automated classifications were broadly consistent with manual classifications that had been made in previous ground surveys, with equivalency in automated and manually derived HMU classes ranging from 61.5% to 87.7%, depending on the river stretch considered. They were found to be discharge-dependent, showing the temporally dynamic aspect of hydromorphology. The proposed system is quick, flexible, generalizable, and provides consistent classifications free from interpretation bias. The deep learning approach used here can be customized to provide more detailed information on flow features, such as delineating between standing waves and advective diffusion of air bubbles/foam, to provide a more refined classification of surface flow patterns, and the classification approach can be further advanced by inclusion of additional remote sensing methods that provide further information on hydromorphological features.

KEYWORDS
aerial orthophotos, CNNs, hydromorphology, LiDAR, mapping

1 | INTRODUCTION

Categorizing fluvial habitat is an essential step for supporting river habitat management and conservation programs. Indeed, the physical habitat composition in a river or stream and the corresponding hydraulic parameters are considered to be basic elements to river health assessment (Maddock, 1999). A range of approaches with associated terminology—*river landform*, *morphological unit*, *mesohabitat type*, *hydromorphological unit* (*HMU*), *physical/hydraulic biotope*, *ecotope*, *channel geomorphic unit* (see Belletti et al., 2017)—have been

developed for categorizing fluvial habitat, reflecting differences in research focus, rationales, and the scale at which the research is conducted. The term "mesohabitat" (e.g., Tickner et al., 2000) applies to a locally contiguous area (typically less than several 100 m in length) consisting of similar hydromorphological conditions, such as flow velocity, turbulence, and depth (see Wegscheider et al., 2020). Pardo and Armitage (1997) characterize mesohabitats as being "visually distinct units of habitat within the stream, recognizable from the bank and with an apparent physical uniformity." Mesohabitats are often associated with particular depth-velocity conditions (Kemp et al., 1999) and it is these interactions between flow and physical habitat characteristics that create the variety of mesohabitats. In particular, surface flow type is considered a major descriptor of physical habitats. The composition and particular assemblage of mesohabitats in a river is an indicator of conditions for fish, macroinvertebrates, and other river biota. Fausch et al. (2002) advocated for the pertinence of mesohabitat characterization for the study of fish ecology, arguing that features relevant to fish movement and behavior, as well as barriers and obstacles, were best assessed at this scale. Mesohabitats are usually defined as distinct classes, such as riffle, glide, pool or run, to cite a few (see, e.g., Parasiewicz, 2007). There is some inconsistency in how mesohabitat types are defined (Newson & Newson, 2000), but typically, these classes compartmentalize a continuum of overall hydromorphological conditions, from slower and more laminar flows in low gradient areas (e.g., glides), to faster and more turbulent flows in higher gradient areas (e.g., rapids). The term *HMU* is often used as a synonym for mesohabitat (Alcaraz-Hernandez et al., 2011; Suska & Parasiewicz, 2020), but in the current study we define this as a broad class, based on the flow features and gradient of the water surface.

A range of methods for classifying fluvial hydromorphology and mesohabitats exist (see Harby et al., 2004 for a first summary and overview), ranging from simple field-based qualitative assessment (e.g., the *River Habitat Survey* method [Newson et al., 1998]; the *Norwegian Mesohabitat Classification Method* [Borsany, 2006; Borsányi et al., 2004]) to numerical modeling approaches (e.g., *MesoCASiMir* [Eisner et al., 2005, 2007], *MesoHabsim* [Parasiewicz, 2007]). Field-based mesohabitat classification may simply involve observing features such as surface flow type from the riverbank and inferring the habitat types from these. For example, in Norway, Borsany (2006) developed a system based on surface flow features or types, surface gradient, flow velocity and depth, all of which can be visually assessed in the field. Such a system requires no specialized instrumentation and can be done using bankside observations, possibly supplemented with qualitative interpretation of aerial photographs. The diversity of methods for identification of mesohabitats in the field has four major difficulties in common: (1) They require some training to provide consistent and robust results; (2) Researcher variability may lead to the same mesohabitat being characterized differently depending on the surveyor; (3) The same mesohabitat type may be identified differently depending on the method used, and similar terms are used by different methods to identify different features; (4) They can be time-consuming depending on the method used and length of river to be surveyed. Numerical modeling approaches, for instance hydraulic modeling, may remove some of the subjectivity but can be very time-consuming, both in terms of obtaining data for model validation and for setting-up the model. Given this, models may benefit from calibration and sensitivity analysis (Franceschini et al., 2019; Martinez-Capel et al., 2016).

Remote sensing, typically based on airborne or satellite true color or multispectral imagery and/or LiDAR data, offers the advantage of providing synoptic coverage of the river at a range of spatial scales pertinent to the mesohabitat and over larger distances. Remote sensing is particularly useful as a source of empirical data for numerical models. For instance, channel bathymetry may be derived from a range of methods (Sundt et al., 2022), and such data can then be used to derive flow properties and other habitat metrics, either by empirical-based hydraulic rules (Hugue et al., 2016) or by hydraulic models (Hauer et al., 2009; Sundt et al., 2022). For example, Hauer et al. (2009) used a rule-based system to classify a watercourse into distinct mesohabitat types (riffles, fast runs, runs, pools, shallows, backwaters) based on predictions from a hydraulic model calibrated using LiDAR data. Drawbacks and limitations to this approach are that establishing hydraulic properties is time-consuming and requires specific expertise. It may also not always be possible to use remote sensing to obtain depth estimates, for instance if the river bottom is not visible in aerial images and/or LiDAR data are unavailable.

Remote sensing may be used to directly determine hydromorphology and mesohabitat because properties of the river's water surface, detectable from remote sensing, are linked to hydromorphology (see Milan et al., 2010). For example, a smooth or rippled water surface may indicate more laminar flows (associated with glide or run mesohabitats). In contrast, standing waves on the surface may indicate the presence of steep channels with coarser bed material: broken standing waves, where the wave breaks and white water is present, being associated with rapids or cascade mesohabitats; and unbroken standing waves, where there is no broken water, being associated with riffle mesohabitats (Faro et al., 2022; Newson & Newson, 2000). Use of surface characteristics has now been incorporated into river science workflows, ranging from mapping surface flow types (Woodget et al., 2016) to mapping mesohabitat (Demarchi et al., 2016). The advantage of deriving hydromorphology directly from remote sensing is that it is possible to retain the primary advantage of remote sensing (synoptic coverage) without the requirement to introduce subsequent modeling (e.g., hydrodynamic modeling). Ideally, the remote sensing approach should be automated to reduce subjectivity and effort.

Automated extraction of information on river habitats from remote sensing imagery is difficult due to a large number of confounding factors (Hedger et al., 2022). Artificial intelligence techniques offer the potential to deal with the complexity existing in imagery of river habitats, and have been used to classify surface cover type (Carbonneau et al., 2020), river sediment sizes (Takechi et al., 2021), hydromorphological features (Rivas Casado et al., 2015), mesohabitats (Milan et al., 2010), and salmon redds (Harrison et al., 2020). There is potential for such an approach to be used to classify features of the water surface (e.g., identifying whether the surface is smooth or whether the surface has standing waves). Flow features identified in such a manner can then be combined with information on surface

gradient (readily obtainable from digital terrain model, DTM, or digital surface model, DSM, data) for a refined hydromorphological classification. Convolutional neural networks (CNNs) are particularly appropriate for this type of work. These are deep learning algorithms that can be trained on images to assign importance (learnable weights and biases) to features of the image within a network linking the images to a predefined classification. A trained network can then be used to predict class types in additional, unclassified images. An effective CNN-based classification of mesohabitat requires the model to be calibrated correctly. Selection of classes may be difficult. An obvious delineation is between smooth/rippled surfaces and those with standing waves. However, river surfaces are often characterized by additional phenomena, such as air bubbles/foam, generated upstream and advectively diffusing downstream (see Chanson, 2012; Schilling & Zessner, 2011). These features have not yet been incorporated into automated mesohabitat mapping systems. This is a limitation because there is potential for a classification system to misidentify diffusing air bubbles/foam, generated by processes upstream, as being broken standing waves, generated by processes beneath the waves. This could lead to mischaracterization of hydromorphology.

Here, we evaluate the potential for automated river classification into HMUs based on airborne remote sensing data. We use a classification system that requires information on only (1) surface patterns, identified by applying a CNN to aerial photographs, and (2) surface gradient, identified from NIR (topographic) LiDAR-derived DTMs, to classify areas of three river stretches, in the Norwegian rivers Alta, Nidelva, and Orkla, into one of four broad HMU classes. These stretches were selected because they offered a range of surface hydromorphological phenomena typical of medium-scale rivers, ranging from smooth or rippled surfaces (in pools, glides, and walks) to standing waves (in splashes, rills, cascades, and rapids). Following Borsányi's rule system (Borsany, 2006), we begin with a simple surface pattern classification (*smooth or rippled* vs. *standing waves*), but we also investigate a more detailed surface pattern classification that allows the distinguishment between standing waves (generated locally) and air bubbles/foam (generated upstream and being advected downstream).

2 | MATERIALS AND METHODS

In the following sections, we describe the procedure for automated HMU classification and its application to selected stretches in three Norwegian rivers. First, we describe the structure of the automated *HMU classification system* (Section 2.1), which uses a Norwegian mesohabitat assessment method based on surface flow pattern (identified by a CNN) and surface gradient. Second, we describe a system—a *Refined surface pattern classification system*—that incorporates an additional surface class ("*diffusing foam*") to better characterize flow features (Section 2.2). We then describe the application of these systems to remote sensing data of the selected river stretches (Section 2.3). All processing was done in R using the *terra* and *insol* libraries, with the exception of the CNN, which was run in python 3.9.7 using TensorFlow 2.9.1 (Joshi et al., 2018) with Keras 2.9.0.

2.1 | HMU classification system

The HMU classification system was devised such that it could classify a river stretch into contiguous cells of preset user-determined dimensions (e.g., 10 × 10 m), where each cell is defined as one of four HMU classes (Figure 1), based on a decision tree using the surface pattern (a feature of the flow) and the surface gradient of the cell. This system is based on the mesohabitat classification system of Borsany (2006), which is commonly used within Norway, but is simplified in that the HMUs are broad in scope, and may include several of Borsányi's mesohabitat types: for example, pools, walks, and glides are within the same HMU. Surface patterns, classified into *smooth or rippled* surfaces and *standing waves*, indicate broad conditions of the flow. HMU classes are defined as:

1. Mild—smooth or rippled. This is characterized by a smooth or rippled surface pattern occurring in a mild surface gradient, and corresponds to the *pool*, *glide*, and *walk* mesohabitat types.
2. Steep—smooth or rippled. This is characterized by a smooth or rippled surface pattern and a steep surface gradient, and corresponds to the *run* mesohabitat type.
3. Mild—standing waves. This is characterized by a standing wave surface pattern and a mild surface gradient, and corresponds to the *splash* and *rill* mesohabitat types.
4. Steep—standing waves. This is characterized by a standing wave surface pattern and a steep surface gradient, and corresponds to the *cascade* and *rapid* mesohabitat types.

The range of mesohabitat types in Borsany (2006) does not include the riffle habitat, but, as characterized in the literature, this can be included in the *mild—standing waves* HMU.

Following Borsany (2006), standing waves were defined as undulations with a height ≥5 cm caused by interaction of the flow and the riverbed in the location of the standing wave and can either be broken (involving "white water") or unbroken (lacking "white water"). *Mild* and *steep* gradients were defined as those with a slope <4% and ≥4%, respectively. Surface patterns and gradients were defined across the river channel within cells of 10 × 10 m, corresponding to 100 × 100 pixels for imagery with a pixel resolution of 0.1 × 0.1 m. This cell size was chosen so that it would be sufficiently large for the CNN to identify differences in pattern among cells, which were dependent on differences in flow. The driving impetus for selecting cell size was to have a sufficient number of pixels for classifying patterns, so the ground size (in meters) was dependent on the spatial resolution of the remote sensing imagery.

Each cell of 100 × 100 pixels was classified as being one of two surface pattern classes—(1) *smooth or rippled*; and (2) *standing waves*—using a CNN constructed using the TensorFlow and Keras libraries (see Lee & Song, 2019). The CNN consisted of two convolution layers (with zero padding), each followed by a pooling layer to down sample the feature maps (Figure 2). Convolution layers and the first dense layer had a rectified linear unit (relu) activation function. The training/validation dataset was split into separate training (70% of the data)

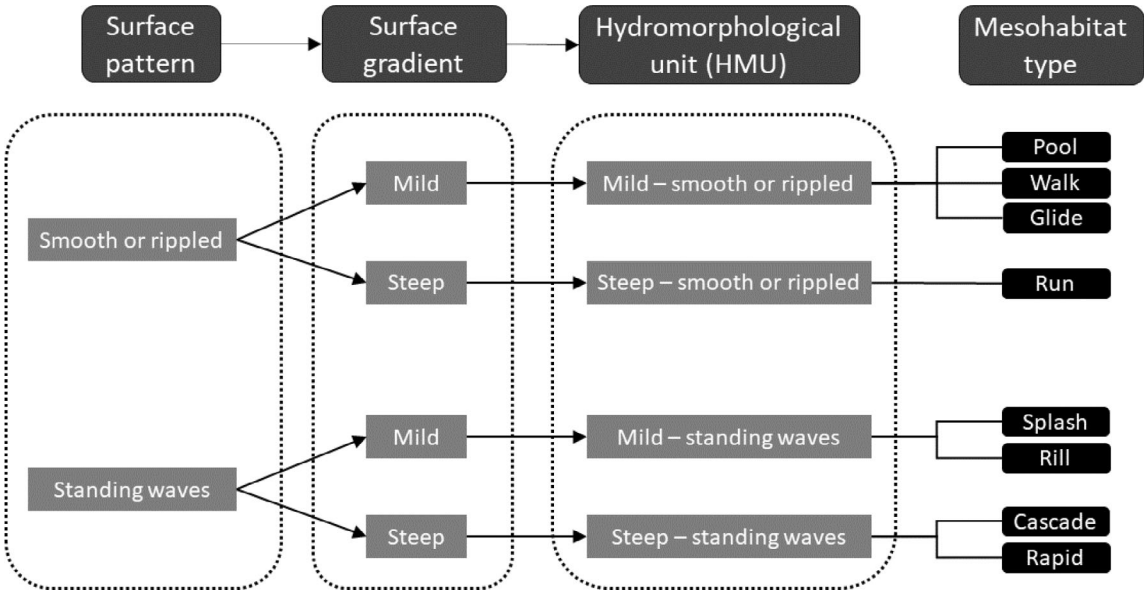

FIGURE 1 Hydromorphological unit classification system structure and associated mesohabitat types. Mesohabitat types are listed in Borsany (2006).

and validation (30% of the data) sets using a random approach. The model was compiled using the Adam Optimizer Algorithm, using a sparse cross-entropy loss function with mini batch gradient descent (batch size = 32). Fifteen epochs (number of times the learning algorithm runs through the entire training dataset) were used to train the model: a greater number of epochs was not used as this sometimes led to overfitting models. The models were evaluated using training and validation accuracy and loss curves.

2.2 | Refined surface pattern classification system

To test the ability to refine the surface pattern classification, the CNN was trained with three classes: (1) *smooth or rippled*; (2) *standing waves*; and (3) *diffusing foam*. Both the standing waves and the diffusing foam classes were characterized by unsmooth surfaces, typically with white water. However, standing waves were created locally; for example, waves overlying submerged boulders. The diffusing foam class represented areas where foam at the water surface had been created by upstream turbulence and was diffusing downstream by a process of advection (see Chanson, 2012; Schilling & Zessner, 2011). Model architecture was equivalent to that used in the two-class CNN.

2.3 | Application of the classification systems

2.3.1 | Remote sensing imagery

To classify surface patterns, aerial orthophotos (resolution = 0.1 × 0.1 m) were acquired from *Norge i bilder* (https://norgeibilder.no), an image repository of orthomosaics provided by the Norwegian Mapping Authority in collaboration with the Norwegian Public Roads Administration and the Norwegian Institute of Bioeconomics. The orthophotos had been obtained under differing light conditions, which affected the illumination of flow features (see Section 4.2), so their use provided an indication of the effectiveness of automated mapping using archived orthophotos rather than dedicated aerial surveys conducted under optimal light conditions. To identify gradients, DTMs (resolution = 1 × 1 m, vertical accuracy s.d. = 0.04 m) were obtained from the Høydedata portal (http://hoydedata.no) of the Norwegian Mapping Authority. DSM data, which showed surface elevation including surface objects such as trees and buildings, were also acquired from the Høydedata portal for use in image pre-processing (Section 2.3.2).

CNN training and validation

The CNNs used in the two classification systems—*HMU classification system* and the *Refined surface pattern classification system*—were trained using orthophotos of stretches of the rivers Nausta in central Norway (length = 1370 m, area = 23,900 m^2, imaged on May 17, 2018) and Suldalslågen in south-west Norway (length = 2650 m, area = 58,400 m^2, imaged on June 2, 2020) (Figure 3). River stretches were compartmentalized into cells (100 × 100 pixels representing 10 × 10 m), and those cells showing clear examples of the surface pattern types—*smooth or rippled* (*N* = 279), *standing waves* (*N* = 166), and *diffusing foam* (*N* = 135)—were selected visually for use in training and validation (Figure 2).

CNN prediction

To predict surface patterns from the CNN and classify HMUs, target images were acquired from stretches of the rivers Alta (imaged on August 2, 2011), Nidelva (imaged on April 27, 2019 and August 7, 2020) and Orkla (imaged on June 10, 2014) (Figure 3). Images were

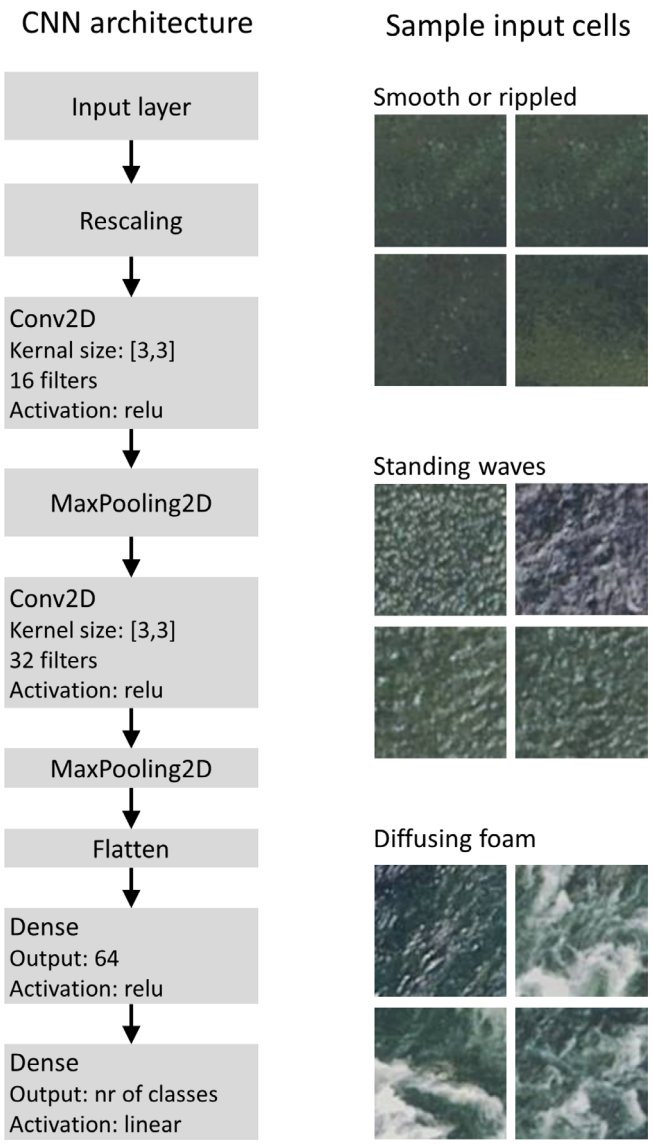

FIGURE 2 Convolutional neural network (CNN) architecture, and sample cell types used in CNN training and validation. Note that the hydromorphological unit classification system only includes the smooth or rippled class and the standing wave class; the refined surface pattern classification system includes all three classes. [Color figure can be viewed at wileyonlinelibrary.com]

selected on the basis of them containing a range of mesohabitats, based on ground surveys that have been previously conducted in these rivers. The imaged stretch of the river Alta (reach length = 2780 m, area = 174,300 m^2, mean width = 63 m) was a mild-gradient meandering reach (mean gradient = 0.23%), with a sequence of areas with smooth or rippled surfaces over deeper waters (glides) and areas with standing waves over shallower waters (splashes). Two images of the river Nidelva were used, one acquired at low discharge and the other at high discharge, to examine how predicted HMUs changed according to discharge. The imaged stretch (reach length = 1090 m, area = 75,500 m^2, mean width = 69 m) had an overall shallow gradient (mean = 0.26%) but consisted of alternating fast turbulent flow mesohabitats with higher gradients (cascades, rapids) and mesohabitats with more laminar flows (pools, walks, glides) in lower gradients (see Borsany, 2006). The imaged stretch of the river Orkla (reach length = 2250 m, area = 183,600 m^2, mean width = 81 m) mainly had a shallow but slightly steeper gradient (mean = 0.62%) than the Alta or Nidelva stretches. It mainly consisted of alternating glides and splashes, with the channel bifurcating around islands, but also included a short cascade in a steeper part of the channel. For assessing the CNN prediction, HMU classes derived from the CNN were compared with the HMU classes manually derived from previously conducted mesohabitat ground surveys. These surveys had been used to derive mesohabitat types based on observations from the bank and/or observations from within the channel using the method developed by Borsany (2006). Surveys in Alta and Orkla were conducted by the Norwegian Institute for Nature Research (see Hindar et al., 2007, 2019), and the survey in the Nidelva was conducted by Borsany (2006). A slight modification was made to the survey classification for the Nidelva, where one mesohabitat that had been initially classified as run mesohabitat was reclassified as a rill based on surface gradient and further survey data. Surface gradient was related to the ground-surveyed mesohabitat types: mean = 0.63% (pool), 0.85% (glide), 1.49% (rill), 1.67% (splash), 2.21% (rapid), 8.97% (cascade) across surveys. Mesohabitat types from these surveys were clustered into the appropriate HMU classes (see Figure 1). Classifications from the automated approach were compared with those from the ground surveys to provide an indication of the "success" of the automated HMU method (i.e., equivalence in HMU classes indicated success).

2.3.2 | Preprocessing of imagery

Surface pattern

Prior to selection of cells used in the CNN (for training and validation, and for prediction), areas outside of the channel and areas that were too dark to observe surface patterns (those under shadow) were removed by masking using the *terra::mask* R function.

- Masking non-channel areas: Channel boundaries were digitized by modifying a polygon database of water bodies across Norway (included in the N50 Kartdata of the Norwegian Mapping Authority; https://www.kartverket.no/api-og-data/kartgrunnlag-fastlands-norge). Areas outside the polygons were then masked, leaving only the wetted channel.
- Masking shaded areas: Shaded areas were identified by visual comparison of shadows in the orthophotos with predicted positions from a shading algorithm (*insol::doshade* R function). Raster maps of shadows were predicted from how the sun would cast shadows based on the elevations of ground surface features (estimated as the difference between the DSM and the DTM elevations) for solar azimuths and elevations on the day of imaging. The raster map of shadows that corresponded best to those in the orthophoto was then used to mask the orthophoto, leaving only the areas under direct sunlight.

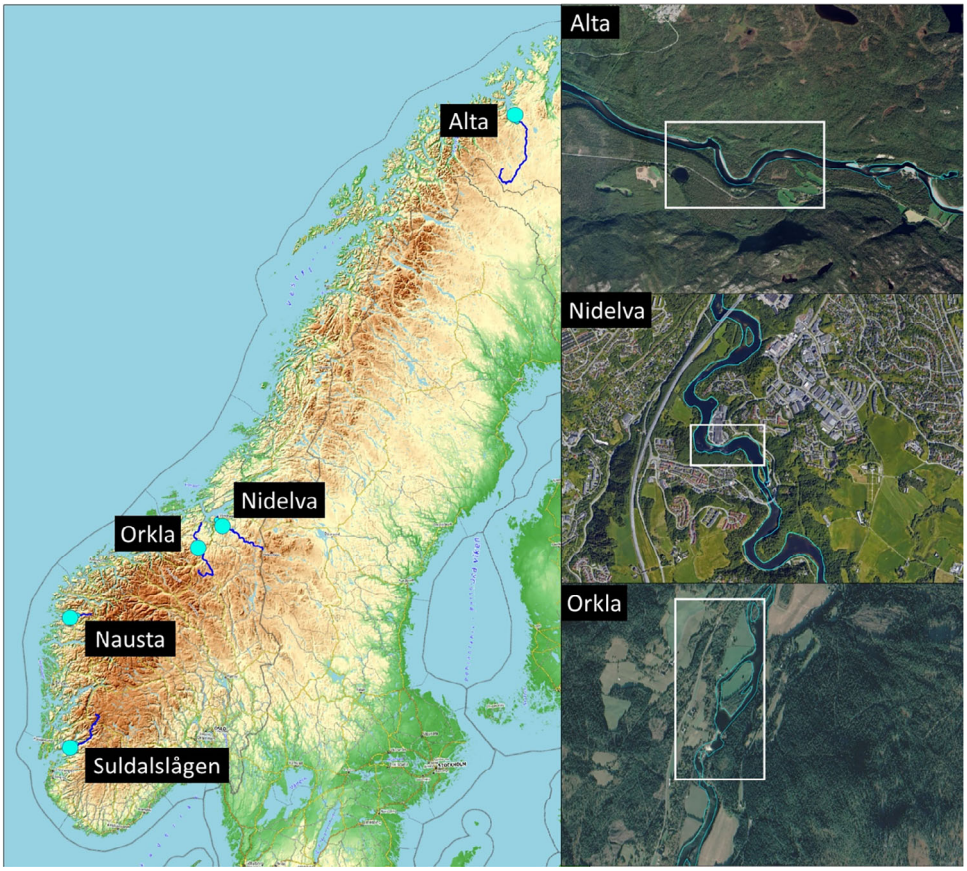

FIGURE 3 Locations of study sites used for training and validation (Nausta and Suldalslågen) and prediction (Alta, Nidelva, and Orkla). Inlet panels show sites used for prediction (white boxes) within the surrounding watercourse. [Color figure can be viewed at wileyonlinelibrary.com]

Surface gradient

Non-channel areas of the DTM were masked by excluding pixels outside of the channel boundary polygon identified in the preprocessing of the aerial orthophotos. The gradient (expressed as a %) for each 1 × 1 m DTM pixel within the channel was estimated by a two-stage procedure: (1) a gradient (in degrees) was calculated using the eight neighboring pixels with the *terra:terrain* R function, and converted to a percentage; (2) this gradient was subsequently smoothed using the *terra:focal* R function (bandwidth = 7 pixels, function = "mean"). The result, referred to as the *surface gradient*, was used in the decision rule framework for automated classification of HMUs.

3 | RESULTS

The training and validation of the CNN for surface pattern classification achieved high accuracies (Figure 3), both for the two-class and the three-class classification. Accuracies were higher for the two-class (≈99%) than the three-class (≈95%) training and validation. Training losses were similar to validation losses, suggesting a reasonable model fit. There was no evidence of overfitting, as validation loss continued to decline with epoch. The change in training loss tended to decline with each successive epoch, but was still gently declining by epoch 15 for the three-class surface classification system, suggesting slight underfitting of the model. However, the CNN performed well when predicting on new datasets, whether based on two classes (Sections 3.1) or three classes (Section 3.2).

3.1 | HMU classification

Overall, the HMU classification system predicted HMUs that were consistent with those that had been identified manually from ground surveys conducted earlier: HMUs derived from the automated approach were equivalent to those of the manual survey classifications in 87.7% (Alta), 81.5% (Nidelva), and 61.5% (Orkla) of cells (see Table S1).

3.1.1 | Alta

The Alta stretch, showing a sequence of alternating slow flowing, *mild—smooth or rippled* HMUs and fast flowing, *mild—standing waves* HMUs (Figure 4; upper panel), was classified into a similar sequence by the automated HMU classification system (Figure 4; middle panel). The gentle gradient of the watercourse (<4%) meant that *steep—smooth or rippled* HMUs (associated with runs) were absent. Only one cell was classified as being *a steep—standing waves* HMU, where the surface gradient locally exceeded 4%: its small size

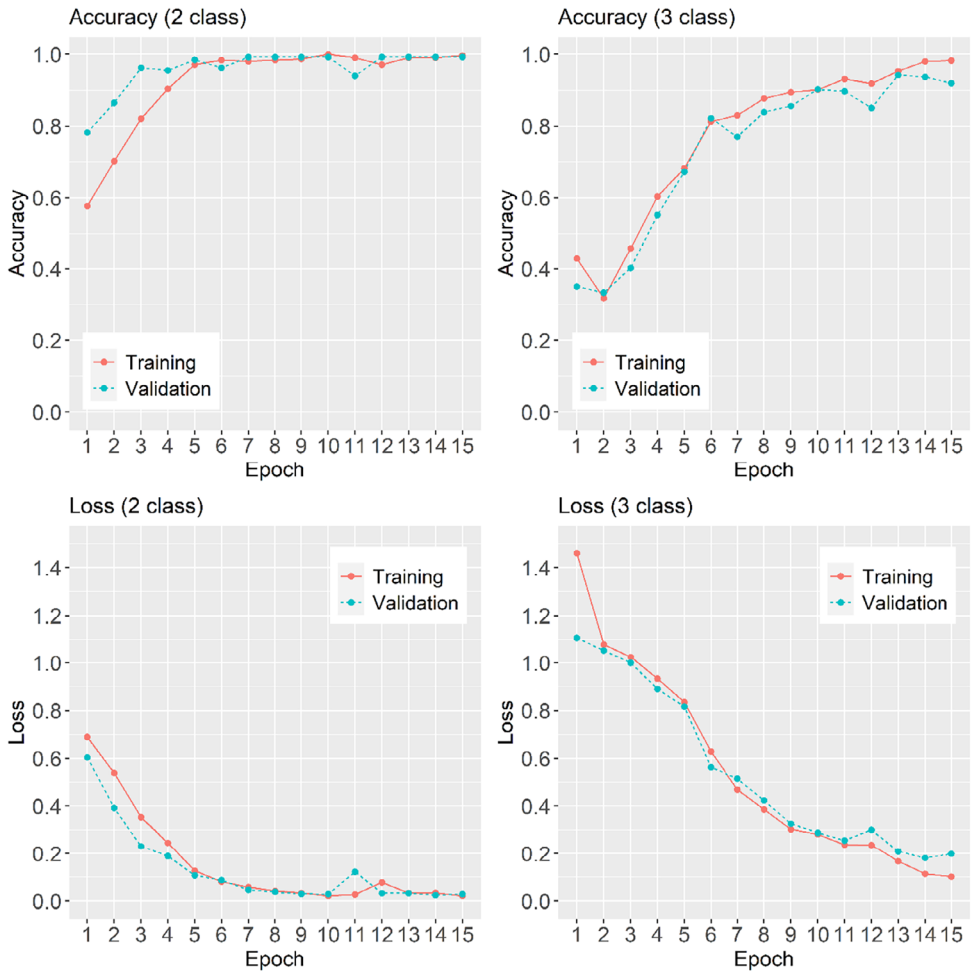

FIGURE 4 Accuracy and loss for training and validation samples in the two-class and three-class surface pattern classification system. Note that the two-class system forms the basis of the hydromorphological unit classification system; the three-class system is the refined surface pattern classification system. [Color figure can be viewed at wileyonlinelibrary.com]

suggests that it is not a functionally "realistic" classification of flow conditions. The automated classification showed a finer level of detail than the manual classification, reflecting the surface patterns identified by the CNN (Figure 4; lower panel). For example, standing waves extended around the outer bank of a meander into an area that had been manually classified into a *mild—smooth or rippled* HMU.

3.1.2 | Nidelva

The automated HMU classification for the Nidelva stretch alternated between mainly *mild—smooth or rippled* and *mild standing waves* or *steep—standing waves* HMUs (Figure 5). *Steep—smooth or rippled* HMUs were rare and only found as isolated cells. The HMUs with more turbulent flows were found in the mid-part of the imaged stretch, where higher gradients occurred (Figure S1). The spatial configuration of mesohabitat types largely concurred with those identified by Borsany (2006) (Figure S1). HMU classifications depended on flow conditions, and the middle parts of the imaged stretch showed an increase in the prevalence of *standing waves* HMUs at high discharge (see inlet panels in Figure 6).

3.1.3 | Orkla

The automated HMU classification of the Orkla stretch was consistent with the manual classification in the mid- to downstream part but diverged from the manual classification in the upstream part (Figure 7). The middle part of the stretch consisted of a smooth water surface in a mild channel gradient (mainly classified as the *mild—smooth or rippled* HMU); the surface became more turbulent further downstream (mainly classified as the *mild—standing waves* HMU). The upstream part of the Orkla stretch consisted of smooth surfaces, separated by short regions of white water associated with rapids or cascades. While the automated HMU classification system was successful in classifying the *mild—standing waves* and *steep—standing waves* areas successfully, it did not, however, always correctly identify areas free from standing waves. For example, some areas were misclassified as *mild—standing waves* HMUs due to the two-class CNN assigning then a *standing wave* classification, when manual examination of the imagery showed the presence of air bubbles/foam rather than standing waves. These misclassifications typically occurred in mild gradient areas, downstream of rapids or cascades where there was white water at the surface from the downstream advective diffusion of air bubbles/foam.

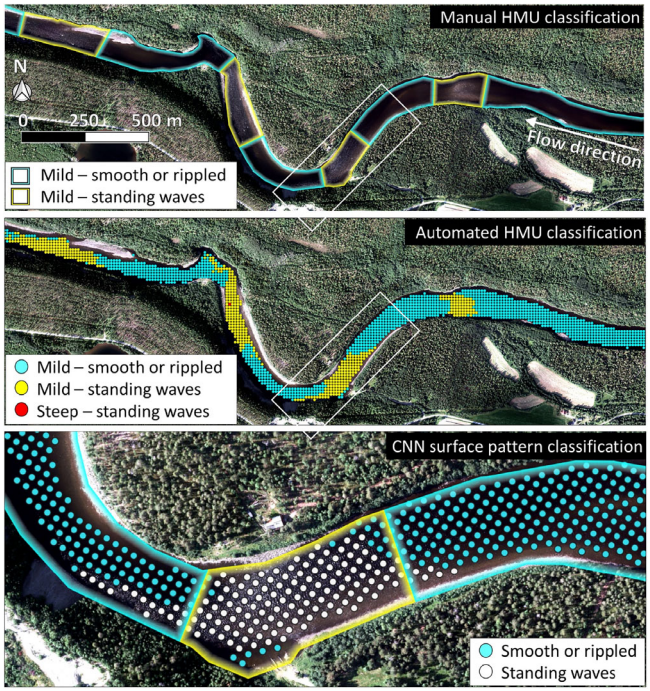

FIGURE 5 River Alta, showing manual and automated hydromorphological unit (HMU) classifications, and surface patterns determined by the convolutional neural network. The white overlaid box on the HMU classifications corresponds to the area covered by the surface pattern panel. [Color figure can be viewed at wileyonlinelibrary.com]

3.2 | Refined surface pattern classification

The refined surface pattern classification system (three classes: *smooth or rippled*, *standing waves*, and *diffusing foam*) classified surface patterns in the Orkla stretch that were consistent with visual inspection of the imagery (Figure 8). In particular, it identified the presence of air bubbles/foam advectively diffusing across pool mesohabitats immediately downstream of rapids. Here, white water was present on the surface but was not in the form of standing waves generated by interaction between the flow and the riverbed immediately beneath the white water. *Smooth or rippled* surface patterns were more prevalent at the downstream side of pools, where surface foam had disappeared due to diffusion.

4 | DISCUSSION

This study has shown that an automated HMU classification system, based on a CNN classification of surface patterns evident in aerial orthophotos, and a rule-based classification of surface gradient based on topographic LiDAR-derived DTMs, can be used to classify river stretches into sections of distinct hydromorphology that are consistent with those identified manually. For the three river stretches examined, classifications broadly coincided with those previously manually identified in ground surveys (Borsany, 2006; Hindar et al., 2019). However, further refinement of the CNN with respect to classification of surface patterns may lead to a better characterization of hydromorphological conditions, particularly with regard to distinguishing between turbulence generated locally (standing waves) and upstream (air bubbles/foam). In the following sections, we discuss the HMU classifications for our study rivers, discuss the sensitivity of the classification to the data used for training and validating the CNN and for making subsequent predictions, and examine how the approach outlined here can be further developed.

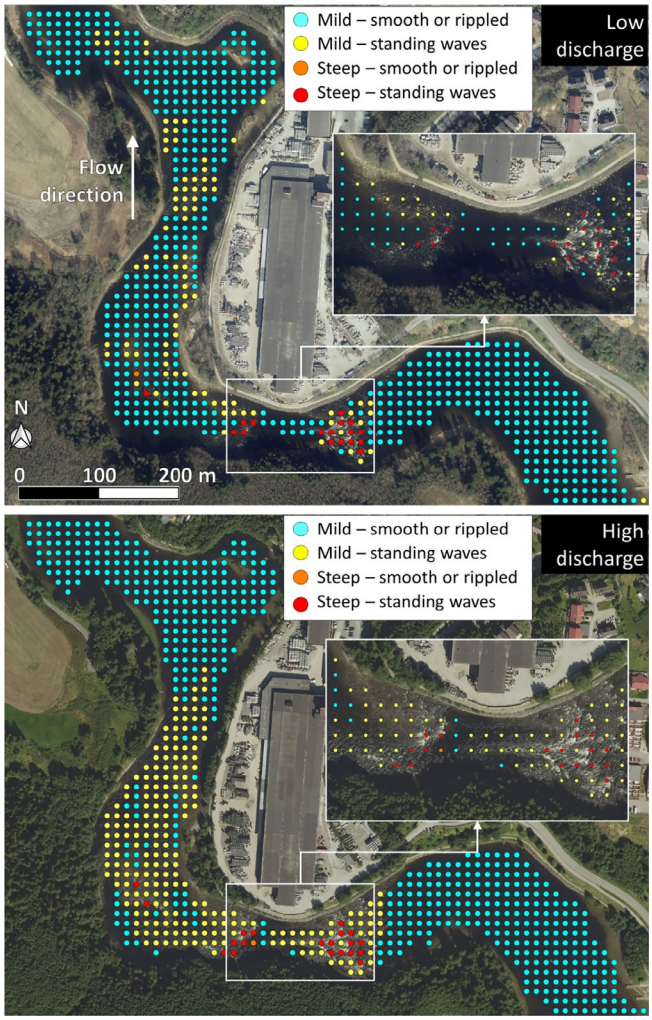

FIGURE 6 Hydromorphological unit classification in the River Nidelva at low and high discharge. [Color figure can be viewed at wileyonlinelibrary.com]

4.1 | HMU classifications in the study rivers

HMU classifications produced by the automated classification system were generally consistent with existing manual classifications based on ground surveys, with the automated HMU classifications coinciding with the manual classifications in 87.7% (Alta), 81.5% (Nidelva), and 61.5% (Orkla) of cells. The automated classification was derived

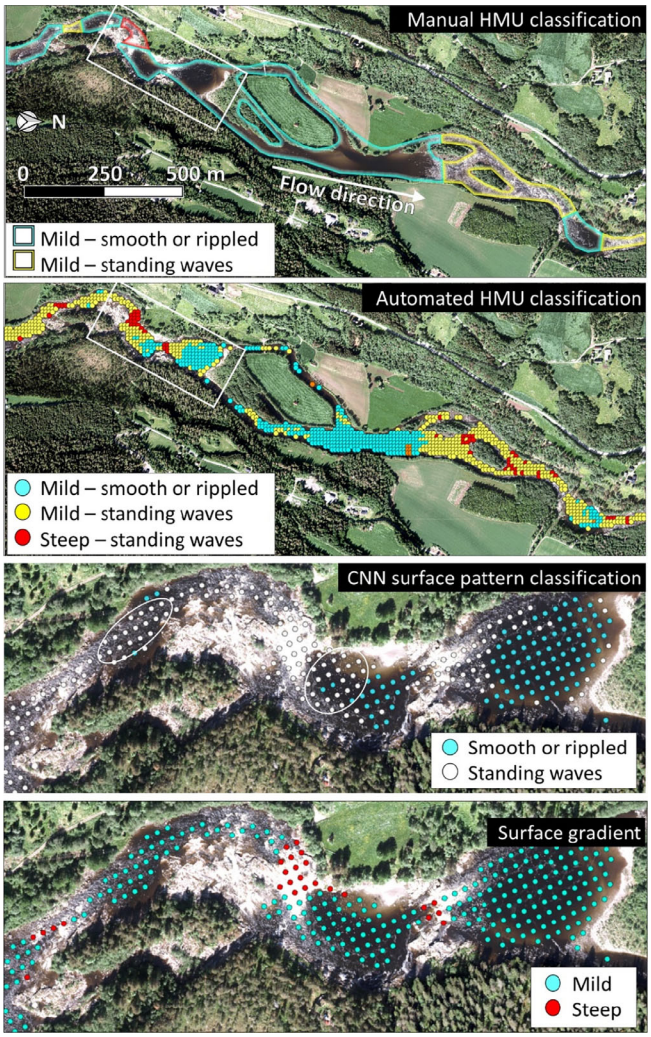

FIGURE 7 River Orkla, showing manual and automated hydromorphological unit classifications, surface patterns determined by the convolutional neural network (CNN) and surface gradient. The white overlaid box on the mesohabitat classifications corresponds to the area covered by the surface pattern and surface gradient panels. Ellipses on the CNN surface pattern classification show areas that are misclassified as standing waves. [Color figure can be viewed at wileyonlinelibrary.com]

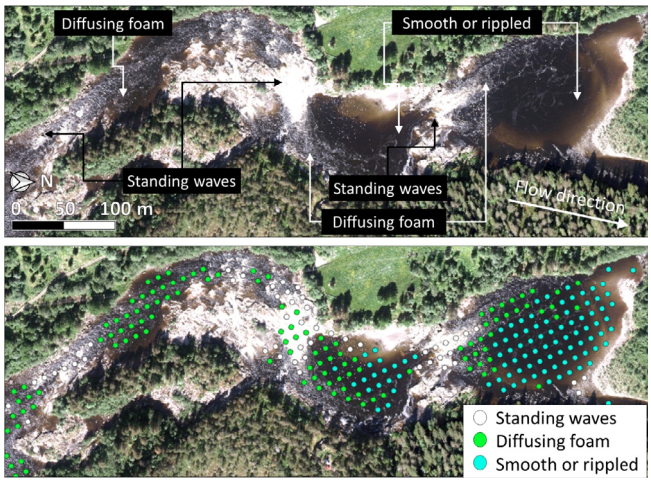

FIGURE 8 River Orkla, showing visually identified surface patterns and refined surface pattern classification. [Color figure can be viewed at wileyonlinelibrary.com]

from the best currently available aerial orthophotos, which were obtained subsequently to when the manual ground surveys of mesohabitat had been made, so may have been based on different flow conditions. Differences between automated and manual classifications may partly be attributed to differences in flow conditions, which are known to affect mesohabitat classifications (Hauer et al., 2009).

No large contiguous area of *steep—smooth or rippled* HMU, associated with the run mesohabitat, was found. Conditions of a smooth or rippled surface pattern alongside a steep gradient are rare in Norway because steep gradients are often associated with standing wave surface patterns; in 16 Norwegian rivers for which manual mesohabitat classifications are available (Alta, Aurland, Eidselva, Enningdalselvam, Flomselvi, Halselva, Imsa, Jolstra, Laerdal, Laerdal, Laukhelle, Nausta, Orkla, Stjorda, Stryn, Suldalslågen; see Hindar et al., 2019), no locations have been classified as corresponding to *steep-smooth or rippled* conditions. The *steep—smooth or rippled* HMU has been identified in other rivers (see Harby et al., 2007) but, overall, appears to be rare. Mesohabitats characterized as being runs are commonly reported, but depending on how the run is defined according to the individual study (e.g., Hauer et al., 2009), may not correspond to the class defined in Borsany (2006). Cases where isolated cells were classified as *steep-smooth* could be argued to be misclassifications, suggesting that it is necessary to set a minimum size for an HMU and/or that the classification should take into account the HMU classifications of the neighboring cells when defining an HMU in any given cell.

The HMU classification was dependent on the surface gradient of the river. We used the 4% threshold of Borsany (2006). However, Borsany (2006) noted, based on expert opinion, that this threshold may be too high for a river reach close to the estuary, such as the Nidelva. The HMU classification did not differentiate between turbulent conditions that were generated locally (standing waves) and the advective diffusion of air bubbles/foam generated upstream. This resulted in inaccurate predictions of hydromorphology in the Orkla in locations downstream of cascades or rapids. These were typically pool habitats, a mesohabitat noted for low turbulence (Stone & Hotchkiss, 2007), which were incorrectly assigned a *mild—standing waves* HMU. A refined surface pattern classification based on three classes correctly classified these areas as *diffusing foam*, suggesting that the HMU classification needs further refinement.

4.2 | Training and validation of the CNN

Key to ensuring an effective hydromorphological classification is using a suitable dataset for training and validating the CNN. The HMU classification system used two very dissimilar classes—*smooth or rippled* versus *standing waves*—so it was easy to train the CNN such that it

could distinguish between these patterns for predicting on new datasets. Additionally, it was easy to create training classes to differentiate between *standing waves* and *diffusing foam*. Differentiating between further unsmoothed conditions (e.g., between broken and unbroken standing waves) requires careful selection of sample classes. This may be difficult because the optical properties of the phenomena may overlap, depending on both local flow conditions and how the imagery is acquired. Training and validation therefore require selection of class examples over a sufficiently broad range of conditions for effective prediction in other river stretches.

The CNN-based approach for identifying flow features is suitable for use with high-resolution aerial photographs of the water surface acquired under appropriate illumination and free of confounding signals, both for training and validating the CNN, and predicting on new datasets. The CNN-based approach relies on imagery with sufficient detail on flow features. In the current study, we used imagery of a 10 cm spatial resolution. Coarse resolutions of the type available through satellite imagery (e.g., 1 m resolution) would probably be insufficient for this. For example, the texture within a stretch of standing waves occurs at short scales (<1 m); integrating this texture at a 1 m resolution would smooth this variation, and potentially make it less distinguishable from smooth or rippled stretches. The CNN-based approach also relies on imagery that are sufficiently illuminated to allow differences between the classes to be detected. The approach may be less effective for identifying mesohabitats when shadows fall across the water surface, making surface patterns less visually identifiable (darker, "noisier" imagery). The approach will therefore be less effective for narrow watercourse headwaters in steep, tree-lined valleys where the entire channel may be obscured by shadow (see Hedger et al., 2022). Additionally, the optical properties of areas in direct sunlight depend on the interaction between the water surface and the solar position (Mount, 2005; Zeng et al., 2017). Surface undulations may be more apparent under direct rather than diffuse sunlight, and specular reflection from unbroken standing waves in imagery taken under direct sunlight could appear more like the white water inherent in broken standing waves. Therefore, the relative frequency of the classification type will depend on the light environment. Finally, the signal from a waterbody is not necessarily solely dependent on surface patterns: in shallow areas, it is possible that the texture on the riverbed from coarse substrates could be confused with surface patterns.

4.3 | Further development and management potential

The method proposed here provides a system by which river surface pattern recognition may be applied to remotely sensed imagery within a decision system to obtain an automated map of river hydromorphology. Automated classification of hydromorphology based on identifying surface flow patterns in remote sensing imagery has received relatively little attention, given the abundant use of CNNs for pattern classification. Surface flow features may be obtained by direct analysis of the 3-dimensional structure of the surface (see Woodget et al., 2016) but such an approach requires a remote sensing technique able to provide this type of information (e.g., using Structure from Motion with UAV imagery). The advantage of the CNN approach used in the current study is that it may be applied to a wide range of imagery (for instance, archived aerial orthophotos which are not necessarily optimal in terms of resolution or image quality for alternative image analysis methods). As such, it has a wider potential for application. Improved application of the remote sensing data may provide a more refined classification: specifically, better characterization of flow features via a refined surface pattern classification, and the use of additional hydromorphological information to refine the habitat classification.

4.3.1 | Refining the surface pattern classification

The HMU classification system only categorized surface patterns into two classes: (1) *smooth or rippled* and (2) *standing waves*. We have shown here that there is potential to distinguish between standing waves and the diffusing air bubbles/foam. There is, however, also potential to differentiate between unbroken and broken standing waves. Unbroken standing waves might have alternating bright pixels, associated with reflections on the side of the wave facing the sun, and darker pixels facing away from the sun. Broken standing waves will have more white water distributed randomly in the cell. The channel characteristics influence hydraulics, so more detailed information on the forms of surface flows might be used in further defining the hydromorphology. For example, unbroken standing waves are more associated with riffles whereas broken standing waves are more associated with rapids and cascades (Newson & Newson, 2000).

4.3.2 | Refining HMU classes

The full classification system on which the current work is based (Borsany, 2006) uses depth and velocity to further refine the mesohabitat type: for example, cascades are defined by shallower depths than rapids. Our HMU classification system used class divisions that were only based on surface patterns and gradient, so only provided four broad HMU types. However, extraction of depth via remote sensing is possible, using bathymetric LiDAR (Hugue et al., 2016; Puig-Mengual et al., 2021; Sundt et al., 2022), or analysis of image spectra (Legleiter & Harrison, 2019; Sundt et al., 2021), or Structure from Motion applied to UAV imagery (Dietrich, 2017). Velocity may be determined using large-scale particle image velocimetry, applied to UAV imagery (Detert & Weitbrecht, 2015). There may also be potential for extraction of depth and velocity using a CNN approach applied to the imagery of the type used in this analysis, based on direct properties within the imagery (e.g., the darkness of an area indicating depth, or foam patterns indicating flow speed). Refining the HMU classes with information obtained directly from the imagery will give a more detailed classification of hydromorphology. An additional

refinement may be to use a more complex rule for assigning HMU on the basis of surface gradient. The system on which the current decision tree is based uses a binary decision based on a gradient threshold of 4%. However, comparison of the ground surveyed mesohabitat type with surface gradient showed that gradient varied according to mesohabitat type. Including a decision rule where a range of gradients indicate a specific mesohabitat type may improve the classification.

4.3.3 | Soft classification

The approach used in the current study used a hard classification: that is, the HMU class assigned to each cell was assigned definitively. Biotope boundaries, however, are fuzzy (Legleiter & Goodchild, 2005). An alternative therefore is to use a soft, or fuzzy, classification where class types are not assigned with 100% certitude (see Milan et al., 2010 and examples therein). Such an approach may prove effective. For example, Legleiter and Goodchild (2005) found that results from fuzzy classification, which allowed for a continuous variation of membership among classes, compared favorably with those from a hard, supervised classification.

The methodology outlined here has strong potential for use in river ecosystem management. First, it has wide applicability. It is suitable for use with archived orthophotos, which might be sub-optimal in terms of spatial resolution or image quality, and thus can be applied to already existing datasets in archived repositories. This expands the spatial coverage because it is not necessary to go to the expense of collecting dedicated data, and the potential application to archived orthophotos allows historical hydromorphology to be quantified. Second, the classification is efficient in terms of labor-hours. Rather than requiring researchers to visit the site, all that is required is access to imagery that probably already exists. Finally, using an automated classification system reduces the potential for researcher-subjectivity in interpreting surface patterns. Thus, pattern classifications will be consistent and independent of the biases of different researchers.

5 | CONCLUSION

Here, we present an approach for automated mapping of fluvial hydromorphology from remote sensing imagery. The main advantages of this approach are that it is quick, flexible, applicable to readily available imagery, and classifications follow a strict rule-based system. First, image processing is fast. The approach does not rely on field surveys or hydraulic modeling, both of which are time consuming, and application of an automated decision rule system is potentially faster than qualitatively interpreting images. The method is flexible and can be easily adapted to various criteria. For example, our HMU classification system used a gradient of 4% as a threshold to distinguish between *mild* and *steep* gradients, but this could be adjusted if it is producing results that appear unrealistic, which may be the case for low-lying, downstream reaches. Imagery of the required types (e.g., aerial photographs with a 10 cm resolution) are usually readily abundant. Within a Norwegian context, orthophotos are available for all rivers, and there is a complete high-resolution topographic LiDAR-derived DTM/DSM covering the country. In locations where existing aerial photographs are not available, imagery of a suitable resolution (e.g., 10 cm) can easily be obtained using UAVs. Additionally, a range of national and global data sources exist that can be used for estimating channel surface gradient (e.g., ASTER DEM; see Azizian & Brocca, 2020). Finally, such a system follows a strict rule-based system, and removes the potential for different researchers to differently interpret the same patterns when qualitatively interpreting imagery. It thus means that classifications are consistent among different rivers and that the reasons for the classifications are documented.

ACKNOWLEDGMENTS

This research was funded by FME HydroCen: Norwegian Research Centre for Hydropower Technology (NFR project number 257588), and the Norwegian Institute for Nature Research (NINA) internal research funds.

DATA AVAILABILITY STATEMENT

The data that support the findings of this study are available in Hydromophology at https://github.com/HedgerNINA/Hydromorphology. These data were derived from the following resources available in the public domain: Norge i bilder, https://norgeibilder.no/; Høydedata, https://hoydedata.no/LaserInnsyn2/.

ORCID

Richard D. Hedger https://orcid.org/0000-0003-0236-3289

REFERENCES

Alcaraz-Hernandez, J. D., Martinez-Capel, F., Peredo-Parada, M., & Hernandez-Mascarell, A. B. (2011). Mesohabitat heterogeneity in four mediterranean streams of the Jucar river basin (Eastern Spain). *Limnetica*, *30*, 363–377.

Azizian, A., & Brocca, L. (2020). Determining the best remotely sensed DEM for flood inundation mapping in data sparse regions. *International Journal of Remote Sensing*, *41*, 1884–1906.

Belletti, B., Rinaldi, M., Bussettini, M., Comiti, F., Gurnell, A. M., Mao, L., Nardi, L., & Vezza, P. (2017). Characterising physical habitats and fluvial hydromorphology: A new system for the survey and classification of river geomorphic units. *Geomorphology*, *283*, 143–157. https://doi.org/10.1016/j.geomorph.2017.01.032

Borsany, P. (2006). A classification method for scaling river biotopes for assessing hydropower regulation impacts. Norwegian University of Science and Technology. https://ntnuopen.ntnu.no/ntnu-xmlui/handle/11250/242068

Borsányi, P., Alfredsen, K., Harby, A., Ugedal, O., & Kraxner, C. (2004). A meso-scale habitat classification method for production modelling of Atlantic salmon in Norway. *Hydroecological Applications*, *14*, 119–138.

Carbonneau, P. E., Dugdale, S. J., Breckon, T. P., Dietrich, J. T., Fonstad, M. A., Miyamoto, H., & Woodget, A. S. (2020). Adopting deep learning methods for airborne RGB fluvial scene classification. *Remote Sensing of Environment*, *251*, 112107. https://doi.org/10.1016/j.rse.2020.112107

Chanson, H. (2012). Advective diffusion of air bubbles in turbulent water flows. In S. G. Shiva, C. Gualtieri, & D. T. Mihailovic (Eds.), *Fluid mechanics of environmental interfaces* (p. 40). CRC Press. https://doi.org/10.1201/b13079

Demarchi, L., Bizzi, S., & Piégay, H. (2016). Hierarchical object-based mapping of riverscape units and in-stream mesohabitats using LiDAR and VHR imagery. *Remote Sensing*, *8*, 97. https://doi.org/10.3390/rs8020097

Detert, M., & Weitbrecht, V. (2015). A low-cost airborne velocimetry system: Proof of concept. *Journal of Hydraulic Research*, *53*, 532–539. https://doi.org/10.1080/00221686.2015.1054322

Dietrich, J. T. (2017). Bathymetric structure-from-motion: Extracting shallow stream bathymetry from multi-view stereo photogrammetry. *Earth Surface Processes and Landforms*, *42*, 355–364. https://doi.org/10.1002/esp.4060

Eisner, A., Schneider, M., Kopecki, I., & Wieprecht, S. (2007). Mesohabitat modelling with MesoCASiMiR: Mapping method, modeling approach and applications. 6th International Symposium on Ecohydraulics. Christchurch, New Zealand.

Eisner, A., Young, C., Schneider, M., & Kopecki, I. (2005). MesoCASiMiR-new mapping method and comparison with other current approaches. *COST Action 626 Report*. European Aquatic Modelling Network. Silkeborg, Denmark.

Faro, D., Baumgartner, K., Vezza, P., & Zolezzi, G. (2022). A novel unsupervised method for assessing mesoscale river habitat structure and suitability from 2D hydraulic models in gravel-bed rivers. *Ecohydrology*, *15*(7), e2452. https://doi.org/10.1002/eco.2452

Fausch, K. D., Torgersen, C. E., Baxter, C. V., & Li, H. W. (2002). Landscapes to riverscapes: Bridging the gap between research and conservation of stream fishes. *Bioscience*, *52*, 483–498. https://doi.org/10.1641/0006-3568(2002)052[0483:ltrbtg]2.0.co;2

Franceschini, S., Tancioni, L., Lorenzoni, M., Mattei, F., & Scardi, M. (2019). An ecologically constrained procedure for sensitivity analysis of Artificial Neural Networks and other empirical models. *PLoS One*, *14*(1), e0211445.

Harby, A., Baptist, M., Dunbar, M. J., & Schmutz, S. (2004). State-of-the-art in data sampling, modelling analysis and applications of river habitat modelling. *COST Action 626 Report*. European Aquatic Modelling Network.

Harby, A., Olivier, J. M., Merigoux, S., & Malet, E. (2007). A mesohabitat method used to assess minimum flow changes and impacts on the invertebrate and fish fauna in the Rhone River, France. *River Research and Applications*, *23*, 525–543. https://doi.org/10.1002/rra.997

Harrison, L. R., Legleiter, C. J., Overstreet, B. T., Bell, T. W., & Hannon, J. (2020). Assessing the potential for spectrally based remote sensing of salmon spawning locations. *River Research and Applications*, *36*, 1618–1632. https://doi.org/10.1002/rra.3690

Hauer, C., Mandlburger, G., & Habersack, H. (2009). Hydraulically related hydro-morphological units: Description based on a new conceptual mesohabitat evaluation model (MEM) using LiDAR data as geometric input. *River Research and Applications*, *25*, 29–47. https://doi.org/10.1002/rra.1083

Hedger, R. D., Sundt-Hansen, L., & Foldvik, A. (2022). Evaluating the suitability of aerial photo sur-veys for assessing Atlantic salmon habitat in Norway. *NINA Report 2105*.

Hindar, K., Diserud, O., Hedger, R. D., Finstad, A. G., Fiske, P., Foldvik, A., Forseth, T., Forsgren, E., Kvingedal, E., Robertsen, G., Solem, Ø., Sundt-Hansen, L. E., & Ugedal, O. (2019). Evaluation of methods for second generation spawning targets for Norwegian salmon populations. *NINA Report 1303*.

Hindar, K., Diserud, O. H., Fiske, P., Forseth, T., Jensen, A. J., Ugedal, O., Jonsson, N., Sloreid, S. E., Arnekleiv, J. V., Saltveit, S. J., Sægrov, H., & Sættem, L. M. (2007). Gytebestandsmål for laksebestander i Norge. *NINA Report 226*.

Hugue, F., Lapointe, M., Eaton, B. C., & Lepoutre, A. (2016). Satellite-based remote sensing of running water habitats at large riverscape scales: Tools to analyze habitat heterogeneity for river ecosystem management. *Geomorphology*, *253*, 353–369. https://doi.org/10.1016/j.geomorph.2015.10.025

Joshi, B., Iutzeler, F., & Amini, M. R. (2018). Large-scale asynchronous distributed learning based on parameter exchanges. *International Journal of Data Science and Analytics*, *5*, 223–232. https://doi.org/10.1007/s41060-018-0110-5

Kemp, J. L., Harper, D. M., & Crosa, G. A. (1999). Use of 'functional habitats' to link ecology with morphology and hydrology in river rehabilitation. *Aquatic Conservation-Marine and Freshwater Ecosystems*, *9*, 159–178. https://doi.org/10.1002/(sici)1099-0755(199901/02)9:1<159::Aid-aqc319>3.0.Co;2-m

Lee, H., & Song, J. (2019). Introduction to convolutional neural network using Keras; an understanding from a statistician. *Communications for Statistical Applications and Methods*, *26*, 591–610. https://doi.org/10.29220/csam.2019.26.6.591

Legleiter, C. J., & Goodchild, M. F. (2005). Alternative representations of in-stream habitat: Classification using remote sensing, hydraulic modeling, and fuzzy logic. *International Journal of Geographical Information Science*, *19*, 29–50. https://doi.org/10.1080/13658810412331280220

Legleiter, C. J., & Harrison, L. R. (2019). Remote sensing of river bathymetry: Evaluating a range of sensors, platforms, and algorithms on the upper Sacramento River, California, USA. *Water Resources Research*, *55*, 2142–2169. https://doi.org/10.1029/2018wr023586

Maddock, I. (1999). The importance of physical habitat assessment for evaluating river health. *Freshwater Biology*, *41*, 373–391. https://doi.org/10.1046/j.1365-2427.1999.00437.x

Martinez-Capel, F., Hauer, C., & Muñoz-Mas, R. (2016). Calibration of the mesohabitat evaluation model (MEM) in Austrian and Iberic rivers. *International Symposium on Ecohydraulics*, Melbourne, Australia.

Milan, D. J., Heritage, G. L., Large, A. R. G., & Entwistle, N. S. (2010). Mapping hydraulic biotopes using terrestrial laser scan data of water surface properties. *Earth Surface Processes and Landforms*, *35*, 918–931. https://doi.org/10.1002/esp.1948

Mount, R. (2005). Acquisition of through-water aerial survey images: Surface effects and the prediction of sun glitter and subsurface illumination. *Photogrammetric Engineering and Remote Sensing*, *71*, 1407–1415. https://doi.org/10.14358/pers.71.12.1407

Newson, M. D., Harper, D. M., Padmore, C. L., Kemp, J. L., & Vogel, B. (1998). A cost-effective approach for linking habitats, flow types and species requirements. *Aquatic Conservation-Marine and Freshwater Ecosystems*, *8*, 431–446. https://doi.org/10.1002/(sici)1099-0755(199807/08)8:4<431::Aid-aqc302>3.0.Co;2-w

Newson, M. D., & Newson, C. L. (2000). Geomorphology, ecology and river channel habitat: Mesoscale approaches to basin-scale challenges. *Progress in Physical Geography*, *24*, 195–217. https://doi.org/10.1177/030913330002400203

Parasiewicz, P. (2007). The MesoHABSIM model revisited. *River Research and Applications*, *23*, 893–903. https://doi.org/10.1002/rra.1045

Pardo, I., & Armitage, P. D. (1997). Species assemblages as descriptors of mesohabitats. *Hydrobiologia*, *344*, 111–128. https://doi.org/10.1023/A:1002958412237

Puig-Mengual, C. A., Woodget, A. S., Munoz-Mas, R., & Martinez-Capel, F. (2021). Spatial validation of submerged fluvial topographic models by mesohabitat units. *International Journal of Remote Sensing*, *42*, 2391–2416. https://doi.org/10.1080/01431161.2020.1862433

Rivas Casado, M., Gonzalez, R. B., Kriechbaumer, T., & Veal, A. (2015). Automated identification of river hydromorphological features using UAV high resolution aerial imagery. *Sensors*, *15*, 27969–27989. https://doi.org/10.3390/s151127969

Schilling, K., & Zessner, M. (2011). Foam in the aquatic environment. *Water Research*, *45*, 4355–4366. https://doi.org/10.1016/j.watres.2011.06.004

Stone, M. C., & Hotchkiss, R. H. (2007). Turbulence descriptions in two cobble-bed river reaches. *Journal of Hydraulic Engineering*, *133*, 1367–1378. https://doi.org/10.1061/(asce)0733-9429(2007)133:12(1367)

Sundt, H., Alfredsen, K., & Harby, A. (2021). Regionalized linear models for river depth retrieval using 3-band multispectral imagery and green

LIDAR data. *Remote Sensing*, *13*, 3897. https://doi.org/10.3390/rs13193897

Sundt, H., Alfredsen, K., Museth, J., & Forseth, T. (2022). Combining green LiDAR bathymetry, aerial images and telemetry data to derive meso-scale habitat characteristics for European grayling and brown trout in a Norwegian river. *Hydrobiologia*, *849*, 509–525. https://doi.org/10.1007/s10750-021-04639-1

Suska, K., & Parasiewicz, P. (2020). Application of the Mesohabitat Simulation System (MesoHABSIM) for assessing impact of river maintenance and restoration measures. *Water*, *12*, 3356. https://doi.org/10.3390/w12123356

Takechi, H., Aragaki, S., & Irie, M. (2021). Differentiation of river sediments fractions in UAV aerial images by convolution neural network. *Remote Sensing*, *13*, 16. https://doi.org/10.3390/rs13163188

Tickner, D., Armitage, P. D., Bickerton, M. A., & Hall, K. A. (2000). Assessing stream quality using information on mesohabitat distribution and character. *Aquatic Conservation-Marine and Freshwater Ecosystems*, *10*, 179–196. https://doi.org/10.1002/1099-0755(200005/06)10:3<179::Aid-aqc403>3.0.Co;2-u

Wegscheider, B., Linnansaari, T., & Curry, R. A. (2020). Mesohabitat modelling in fish ecology: A global synthesis. *Fish and Fisheries*, *21*, 927–939. https://doi.org/10.1111/faf.12477

Woodget, A. S., Visser, F., Maddock, I. P., & Carbonneau, P. E. (2016). The accuracy and reliability of traditional surface flow type mapping: Is it time for a new method of characterizing physical river habitat? *River Research and Applications*, *32*, 1902–1914. https://doi.org/10.1002/rra.3047

Zeng, C. Q., Richardson, M., & King, D. J. (2017). The impacts of environmental variables on water reflectance measured using a lightweight unmanned aerial vehicle (UAV)-based spectrometer system. *ISPRS Journal of Photogrammetry and Remote Sensing*, *130*, 217–230. https://doi.org/10.1016/j.isprsjprs.2017.06.004

SUPPORTING INFORMATION

Additional supporting information can be found online in the Supporting Information section at the end of this article.

How to cite this article: Hedger, R. D., & Gosselin, M.-P. (2023). Automated fluvial hydromorphology mapping from airborne remote sensing. *River Research and Applications*, *39*(9), 1889–1901. https://doi.org/10.1002/rra.4186